

## Reflection high-energy electron diffraction from carbon nanotubes

Jason T. Drotar,<sup>1</sup> B. Q. Wei,<sup>2</sup> Y.-P. Zhao,<sup>1</sup> G. Ramanath,<sup>2</sup> P. M. Ajayan,<sup>2</sup> T.-M. Lu,<sup>1</sup> and G.-C. Wang<sup>1</sup>

<sup>1</sup>*Department of Physics, Applied Physics, and Astronomy, Rensselaer Polytechnic Institute, Troy, New York 12180-3590*

<sup>2</sup>*Department of Materials Science and Engineering, Rensselaer Polytechnic Institute, Troy, New York 12180-3590*

(Received 1 May 2001; published 10 September 2001)

Using reflection high-energy electron diffraction, we have observed diffraction patterns from both vertically aligned and randomly oriented multiwalled carbon nanotube samples. The patterns, for both samples, consist of rings and are similar to the patterns observed in x-ray diffraction from multiwalled carbon nanotubes. The ring radii are roughly consistent with powder diffraction from graphite. However, the ratio of the interlayer spacing to the in-plane nearest-neighbor distance is, for both samples, higher than the ordered graphite value of 2.36. Also, reflection electron energy-loss spectra were taken for both samples. For the vertically aligned sample, the center-to-center spacing of the nanotubes was determined, from the energy-loss spectrum, to be  $52 \pm 12$  nm.

DOI: 10.1103/PhysRevB.64.125417

PACS number(s): 61.46.+w, 81.07.De, 61.14.Hg

### I. INTRODUCTION

In recent years, there has been great interest in determining the structural properties of carbon nanotubes. This is important because other aspects of a carbon nanotube (for example, its electrical characteristics) will often be dictated by its structure. So far, people have employed many different methods to determine the structure of nanotubes. Direct imaging methods such as scanning electron microscopy (SEM) and transmission electron microscopy (TEM) have been used to determine the arrangement of nanotube arrays as well as the structure of individual nanotubes.<sup>1-4</sup> Diffraction techniques have also been widely used for determining the structure of nanotubes. For example, x-ray diffraction studies have shown that multiwalled nanotubes consist of shells of graphite with little or no interlayer correlation and that the interlayer spacing is about 2% larger than that for ordered graphite.<sup>4-7</sup> Burian *et al.* found, using neutron diffraction, that some correlation exists among graphite shells of multiwalled nanotubes, and they also observed that the interlayer spacing is about 2% higher than that for ordered graphite.<sup>8</sup> In addition to observing x-ray diffraction patterns from multiwalled carbon nanotubes, Saito *et al.* obtained electron diffraction patterns from a single multiwalled carbon nanotube.<sup>7</sup> Recently, Terranova *et al.* claimed that they observed ring patterns from single-walled carbon nanotubes using reflection high-energy electron diffraction (RHEED).<sup>9</sup> However, it should be pointed out that their measurements were carried out on protruding regions of their sample, with a primary energy of 60 keV (a very high energy for conventional RHEED). Thus it is likely that their measurements actually correspond to transmission electron diffraction.

It is well known that RHEED (with electron energies ranging from 5 to 20 keV) is a powerful instrument for *in situ*, real-time characterization of growth and etching processes in high vacuum and ultrahigh vacuum. It would be very useful if one could apply RHEED to characterize the nanotube formation process, but so far, there have not been any reported studies of multiwalled nanotubes using RHEED. In this paper, we present a detailed study of the structural properties of vertically aligned and randomly oriented multiwalled carbon nanotube samples using energy-

filtered RHEED. By studying the diffraction patterns in detail, we can not only obtain information on the crystal structure of individual nanotubes, but can also characterize the alignment and spacing of the nanotubes. Our results are consistent with results from other studies of multiwalled carbon nanotubes.

### II. EXPERIMENT

The multiwalled nanotube samples were prepared using the chemical vapor deposition (CVD) method. The substrate, in each case, was Si(001) capped with a 100-nm thermally grown oxide layer, and the nanotubes were grown by exposing the substrate to xylene and ferrocene for 15 min at 800 °C. Both a vertically aligned sample and a randomly oriented sample were prepared. The vertically aligned sample was produced by increasing the amount of xylene used (compared to the amount used for the randomly oriented sample) and, hence, the amount of carbon. The ratio of xylene to ferrocene was about 10 to 1 for the randomly oriented sample and 90 to 1 for the vertically aligned sample. The alignment of the as-grown samples was investigated by SEM. The SEM images (Fig. 1) show that the nanotubes in the vertically aligned sample are fairly straight and point in roughly the same direction, while the randomly oriented sample contains a disordered tangle of nanotubes.

The diffraction experiment was carried out in a stainless steel chamber (at a pressure of about  $1 \times 10^{-8}$  Torr) equipped with a 15-keV RHEED gun that can produce a 100- $\mu$ m spot. High-energy electrons are incident on the sample at an angle of about 1°, and the diffracted electrons pass through two metal grids before striking a phosphor screen. The resulting diffraction pattern is imaged using a 16-bit Princeton Instruments charge-coupled device (CCD) camera. To improve the signal-to-noise ratio, the CCD camera is cooled to  $-30$  °C before image acquisition.

The two metal grids constitute an energy filter, which is used for acquiring energy-loss spectra. The filter follows a design similar to that of Braun,<sup>10</sup> and both grids are made of 500-line-per-inch nickel, with an open area that is about 60% of the total area. Both the first grid (the one farthest from the phosphor screen) and the phosphor screen are kept grounded.

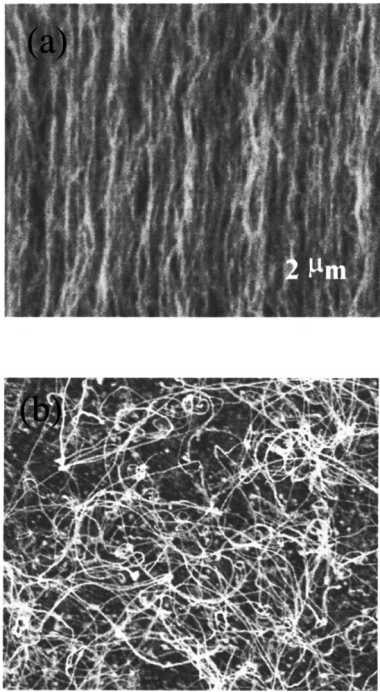


FIG. 1. Scanning electron microscope (SEM) images of (a) vertically aligned and (b) randomly oriented multiwalled nanotube samples. The scale is the same for both images.

When conventional RHEED (no energy filtering) patterns are acquired, the second grid (also called the suppressor grid) is also grounded. However, when acquiring energy-loss spectra, the second grid is kept at the primary RHEED voltage (which is negative) plus a small (0–100 V) positive offset, and only electrons with sufficient energy can pass this grid. Those that do pass the second grid are reaccelerated before striking the phosphor screen. By sweeping the voltage on the second grid and measuring the diffraction intensity, an energy-loss spectrum can be acquired.

Due to the curved path that the electrons take through the energy filter, there is some distortion of the energy-filtered diffraction patterns. However, we have found that the amount of distortion is negligible. A more serious problem is the fact that the energy cutoff of the filter varies with position. The difference in cutoff can be as much as 25 V from one point to another and is due mainly to wrinkles in the second grid (caused during assembly of the grid). The problem is overcome by taking a series of images at different suppressor voltages and determining the cutoff from the position of the elastic peak. In this manner, the cutoff can be determined pixel by pixel and subsequently accounted for.

### III. RESULTS AND DISCUSSION

#### A. RHEED patterns

RHEED patterns for both the vertically aligned and randomly oriented samples are shown in Fig. 2. The patterns, for both samples, consist of concentric rings whose radii are roughly consistent with powder diffraction from graphite. This is expected since multiwalled carbon nanotubes are

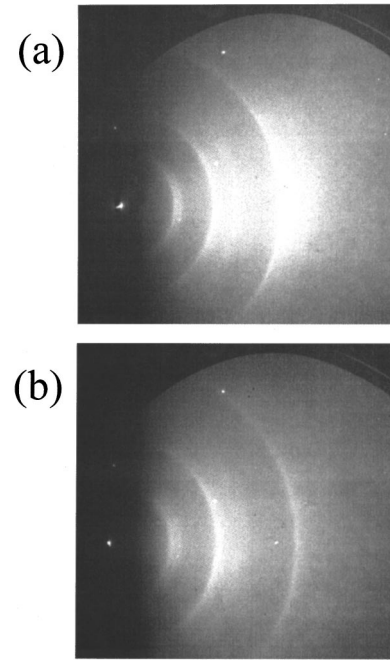


FIG. 2. Reflection high-energy electron diffraction (RHEED) images of the (a) vertically aligned and (b) randomly oriented multiwalled nanotube samples. The primary electron energy used was 11 keV for the vertically aligned sample and 8 keV for the randomly oriented sample. Each image consists of  $512 \times 512$  pixels, and the grayscale corresponds to intensity. Neither image was energy filtered, but there are still several bright spots caused by defects in the energy filter grids.

simply concentric tubes of cylindrically rolled graphite layers, as shown in Fig. 3. The carbon atoms of a single graphite layer follow a hexagonal pattern. For ordered graphite, the hexagonal lattice of each layer is shifted a distance  $a$  with respect to adjacent layers. The primitive lattice vectors for such a structure are given by

$$\mathbf{x} = \left( \frac{-3a}{2}, \frac{\sqrt{3}a}{2}, 0 \right), \quad \mathbf{y} = (0, -\sqrt{3}a, 0), \quad \mathbf{z} = (0, 0, 2b), \quad (1)$$

and the lattice has basis atoms at  $(0, 0, 0)$ ,  $(-a, 0, 0)$ ,  $(0, 0, b)$ , and  $(a, 0, b)$ . The reciprocal lattice vectors are given by

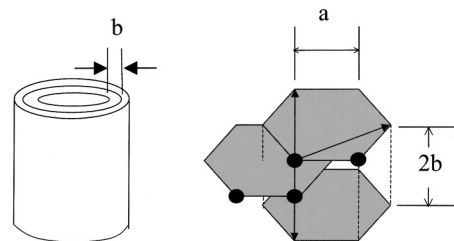


FIG. 3. Structure of a multiwalled carbon nanotube. The layers are separated by a distance  $b$ . Each layer, when unrolled, consists of a two-dimensional hexagonal lattice of carbon atoms, with a lattice constant  $a$ .

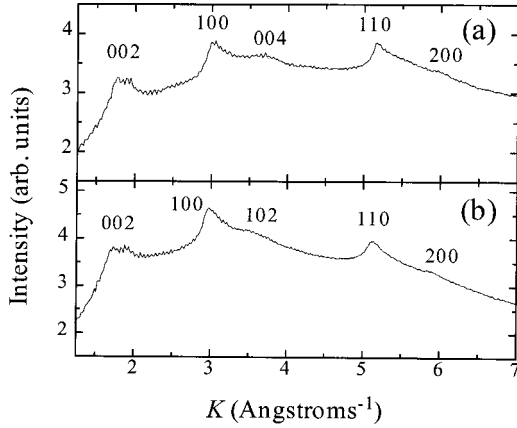


FIG. 4. Radial profile of the diffraction intensity for the (a) vertically aligned sample and (b) randomly oriented sample. Since a given radial distance corresponds to a given momentum transfer  $K$ , the radial distances have been converted from pixels to  $\text{\AA}^{-1}$ .

$$\mathbf{k}_x = 2\pi \left( \frac{-2}{3a}, 0, 0 \right), \quad \mathbf{k}_y = 2\pi \left( \frac{-1}{3a}, \frac{-1}{\sqrt{3}a}, 0 \right),$$

$$\mathbf{k}_z = 2\pi \left( 0, 0, \frac{1}{2b} \right), \quad (2)$$

and any point in the reciprocal lattice can be written as

$$\mathbf{G} = h\mathbf{k}_x + k\mathbf{k}_y + l\mathbf{k}_z, \quad (3)$$

where  $h$ ,  $k$ , and  $l$  are integers. Because the lattice has more than one basis atom, the diffraction intensity will vary from point to point. If we ignore the atomic form factor, the diffraction intensity is given by

$$I(h, k, l) = 2 + 2 \cos \left( 2\pi \left[ \frac{h-k}{3} \right] \right) + 2 \cos \left( 2\pi \left[ \frac{h-k}{3} + \frac{l}{2} \right] \right) + \cos \left( 2\pi \left[ \frac{2(h-k)}{3} + \frac{l}{2} \right] \right) + \cos(\pi l). \quad (4)$$

Note that certain points in the reciprocal lattice will have zero intensity. If the RHEED patterns corresponded to powder diffraction from ordered graphite, then we would expect a ring for each set of  $hkl$  for which  $I(h, k, l)$  does not vanish.

### B. Radial profiles of rings and lattice parameters

In order to quantitatively determine the ring radii, radial profiles of the diffraction patterns for both the vertically aligned and randomly oriented samples are shown in Fig. 4. A radial profile is found by averaging the intensities of pixels with the same distance  $r$  (to within 1 pixel) from the center of the rings. The task of determining ring positions is complicated by the fact that certain rings are very close together. This makes it difficult to determine how many rings there actually are, because a weak ring can be obscured by a stronger nearby ring. Looking at the RHEED images in Fig. 2, one can clearly see three major rings. However, the first ring looks as if it could actually be two rings. Also, looking at Fig. 4, it appears that the second and third major rings may

be accompanied by weaker rings. The parameter  $b$  can be found by looking at the radius of the (002) ring (the first major ring), while the parameter  $a$  can be found by looking at the radius of the (100) ring (the second major ring). For the vertically aligned sample, we found that  $a = 1.37 \pm 0.06 \text{ \AA}$  and  $b = 3.41 \pm 0.15 \text{ \AA}$ , while for the randomly oriented sample, we found that  $a = 1.41 \pm 0.06 \text{ \AA}$  and  $b = 3.44 \pm 0.15 \text{ \AA}$ . The large error is due to uncertainty in the sample to screen distance. For ordered graphite,  $a = 1.42 \text{ \AA}$  and  $b = 3.35 \text{ \AA}$ . For multiwalled nanotubes, the values  $\sqrt{3}a = 2.468 \pm 0.01 \text{ \AA}$  (corresponding to  $a = 1.425 \pm 0.006 \text{ \AA}$ ) and  $b = 3.442 \pm 0.01 \text{ \AA}$  have been observed using x-ray diffraction.<sup>7</sup> Given the large error bars for our data, it is impossible to say with certainty whether the actual values for  $a$  and  $b$  differ from the values for ordered graphite. However, we can determine the ratio  $b/a$  with greater accuracy. (A change in the sample-to-screen distance will not affect the ratio  $b/a$ .) In Table I, we list observed values for  $a$ ,  $b$ , and  $b/a$ . It is clear that for both the vertically aligned and randomly oriented samples, the ratio  $b/a$  is larger than the value for ordered graphite.

In Table II, we list the expected ring radii for an ordered graphite structure with  $a$  and  $b$  equal to the values measured from each nanotube sample. Also shown are the measured radii for the observed rings. Since  $a$  and  $b$  were determined from the (100) and (002) rings, respectively, the measured radii for these rings will obviously be equal to the expected radii. For the other rings, there is also good agreement between the expected and measured values, and in each case, the measured value is within 2% of the expected value. Of course, one should keep in mind that some of the peaks are quite small and spread out, making it difficult to tell exactly where the peak is. Another issue is the fact that not all rings are observed. From Table II, one can see that  $I(h, k, l)$  vanishes for some rings, and as expected, these rings are not observed. However, even if we ignore the rings for which  $I(h, k, l)$  vanishes, there are still many other rings that are not observed. One possibility is that the nanotube layers might not be arranged as in ordered graphite. In fact, it has been observed that, in multiwalled nanotubes, there is little or no correlation between layers.<sup>5-7</sup> For such a case, one would expect only rings of the form  $(hk0)$  or  $(00l)$ . For the vertically aligned sample, this appears to be the case. The absence of a (006) ring is a little odd, but this ring is probably just obscured by the (110) and (200) rings. For the randomly oriented sample, both the (004) and (006) rings are missing. Most likely, these rings are also obscured by nearby rings. However, the existence of a (102) ring suggests that there is at least some correlation between adjacent layers.

An interesting feature of the observed rings is the asymmetry in the radial intensity profile of each ring. For a graphite structure with no interlayer correlation (turbostratic), we would expect asymmetry only for rings of the form  $(hk0)$ . This is due to the fact that, for such a structure, reciprocal lattice points of the form  $(hk0)$  are smeared out in the  $z$  direction to form rods. For the case of powder diffraction, this reciprocal-space structure is averaged over all possible orientations. Reciprocal-space points become spheres. Reciprocal-space rods that do not pass through the origin

TABLE I. Observed values for  $a$ ,  $b$ , and  $b/a$  for multiwalled carbon nanotubes. The observed degree of interlayer correlation is also noted.

	$a$	$b$	$b/a$	Interlayer correlation	Reference
Ordered graphite	1.42	3.35	2.36	Perfect	
Vertically aligned sample	$1.37 \pm 0.06 \text{ \AA}$	$3.41 \pm 0.15 \text{ \AA}$	2.49	None	This work
Randomly oriented sample	$1.41 \pm 0.06 \text{ \AA}$	$3.44 \pm 0.15 \text{ \AA}$	2.44	Almost none	This work
X-ray diffraction study of Jin, Bower, and Zhou		3.41 $\text{ \AA}$			4
X-ray diffraction study of Reznik <i>et al.</i>		3.42 $\text{ \AA}$		Short ranged	5
X-ray diffraction study of Zhou <i>et al.</i>		$3.44 \pm 0.09 \text{ \AA}$		Short ranged	6
X-ray diffraction study of Saito <i>et al.</i>	$1.425 \pm 0.006 \text{ \AA}$	$3.442 \pm 0.01 \text{ \AA}$	2.42	None	7
Electron diffraction study of Saito <i>et al.</i>			2.42		7
Neutron diffraction study of Burian <i>et al.</i>	$1.41 \pm 0.01 \text{ \AA}$	$3.41 \pm 0.01 \text{ \AA}$	2.42	Short ranged	8

yield a spherical intensity distribution that begins abruptly for a given  $r$  (corresponding to the point of closest approach to the origin) and decreases for larger values of  $r$ . From Fig. 4, we see clear asymmetry for rings of the form  $(hk0)$ , but rings of the form  $(00l)$  also have some asymmetry. The asymmetry of these rings could be from the high background intensity of the RHEED patterns or from intensity contributions from adjacent peaks.

### C. Orientation of nanotubes

In principle, the RHEED patterns can also contain information about the orientation of the nanotubes. For the randomly oriented sample, all possible orientations are realized, so the reciprocal space should consist of spheres. In this case, one would naively expect a diffraction pattern consisting of rings with uniform intensity. In Fig. 5, we plot the angular intensity profile along the  $(002)$  ring for both the vertically

TABLE II. Expected and measured ring radii for the vertically aligned and randomly oriented nanotube samples.

$(hkl)$	Vertically aligned sample		Randomly oriented sample		$I(h,k,l)$
	Expected ring radius ( $\text{\AA}^{-1}$ )	Measured ring radius ( $\text{\AA}^{-1}$ )	Expected ring radius ( $\text{\AA}^{-1}$ )	Measured ring radius ( $\text{\AA}^{-1}$ )	
(001)	0.92		0.91		0.0
(002)	1.84	1.84	1.83	1.83	8.0
(003)	2.76		2.74		0.0
(100)	3.05	3.05	2.98	2.98	0.5
(101)	3.18		3.11		1.5
(102)	3.56		3.49	3.50	0.5
(004)	3.68	3.70	3.65		8.0
(103)	4.11		4.04		1.5
(005)	4.60		4.56		0.0
(104)	4.78		4.71		0.5
(110)	5.28	5.19	5.15	5.14	8.0
(111)	5.36		5.23		0.0
(006)	5.52		5.48		8.0
(112)	5.59		5.47		8.0
(113)	5.96		5.84		0.0
(200)	6.10	6.00	5.95	5.86	0.5

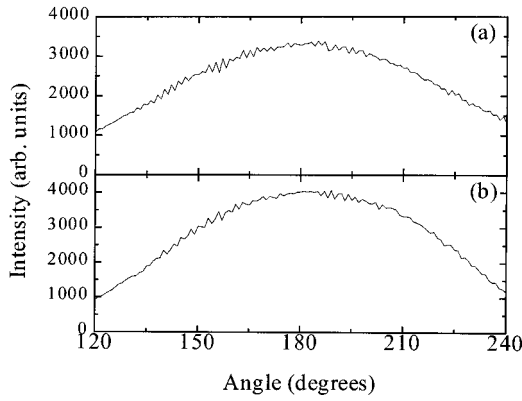


FIG. 5. Angular profile of the diffraction intensity along the (002) ring for the (a) vertically aligned sample and (b) randomly oriented sample. The direction indicated by  $90^\circ$  points straight upward, while the direction indicated by  $180^\circ$  points directly to the right (see Fig. 2).

aligned and randomly oriented samples. Surprisingly, the intensity for the randomly oriented sample is not uniform, but this is probably due to multiple scattering. While one would expect a uniform profile for the randomly oriented sample, one would expect a profile with sharp peaks at  $90^\circ$  and  $270^\circ$ , for the vertically aligned sample. Actually, since the RHEED images contain information for only a limited range of angles (which does not contain  $90^\circ$  or  $270^\circ$ ), one would not even expect to have a (002) ring for the vertically aligned sample. However, the nanotubes in the vertically aligned sample are not perfectly aligned, and the sample could even have regions with randomly oriented nanotubes. Furthermore, there could be disorder present in individual nanotubes. In Fig. 6, we plot the angular profile of the intensity ratio between the vertically aligned and randomly oriented samples along the three major rings. The intensity ratio for the (002) profile tends to increase as one goes toward  $90^\circ$  or  $270^\circ$ , indicating the existence of a preferred direction in the vertically aligned sample. The (100) and (110) profiles are relatively flat.

#### D. Energy-loss spectra and nanotube center-to-center spacing

To obtain additional information about the nanotubes, energy-loss spectra were acquired for both the vertically

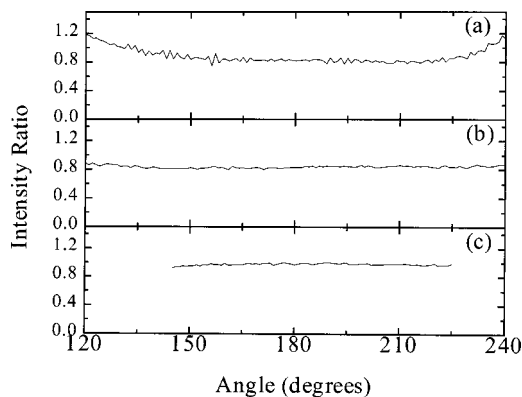


FIG. 6. Angular profiles of the intensity ratio between the vertically aligned and randomly oriented samples along (a) the (002) ring, (b) the (100) ring, and (c) the (110) ring.

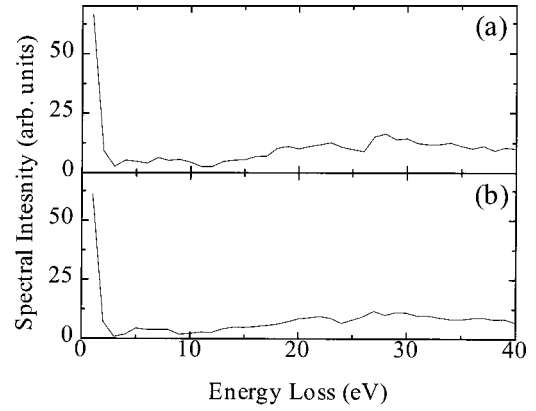


FIG. 7. Electron energy-loss spectra (EELS) for the (a) vertically aligned sample and (b) randomly oriented sample. The primary energy, in both cases, was 8 keV.

aligned and randomly oriented samples. The spectra were obtained by measuring the intensity at the middle of the (002) ring for different suppressor grid voltages (corresponding to different energy losses). The actual spectral intensity is the derivative (with respect to energy loss) of the measured intensity, and the spectra are shown in Fig. 7. For each sample, the spectrum consists of a large elastic peak followed by a diffuse inelastic part. It is important to note that, in addition to having a lower energy, an inelastically scattered electron will have a smaller momentum. This is shown in Fig. 8. The diffraction intensity will depend both on the energy loss  $E$  and the momentum transfer  $\mathbf{K} = \mathbf{k}_{\text{out}} - \mathbf{k}_{\text{in}}$ . For simplicity, we assume that the intensity can be written as

$$I = I_E(E)I_K(\mathbf{K}). \quad (5)$$

While this assumption might not always hold, it should at least be true for a limited range of  $E$  and  $\mathbf{K}$ . If we could divide out  $I_E$ , then we would be able to obtain structural

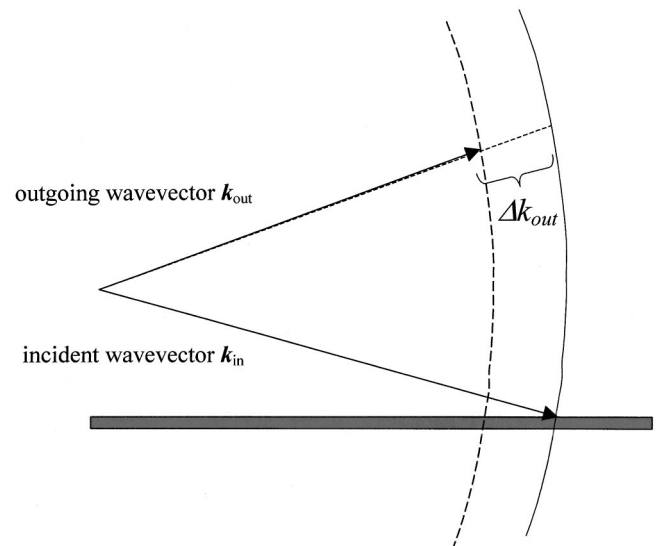


FIG. 8. Ewald construction for electron diffraction with inelastic scattering. In addition to a lower energy, the outgoing electron has a smaller momentum than the incoming electron.

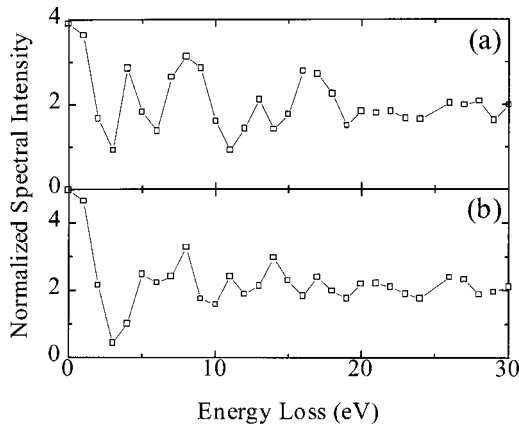


FIG. 9. Normalized electron energy-loss spectra for the (a) vertically aligned sample and (b) randomly oriented sample.

information about the surface from the energy-loss spectrum. In principle,  $I_E$  can be found by obtaining an energy-loss spectrum from a place in the diffraction pattern where  $I_K$  varies slowly as a function of  $\mathbf{K}$ . The area beyond the (110) ring should satisfy this criterion, because the component of  $\mathbf{K}$  perpendicular to the surface is large in that area.

In Fig. 9, we show energy-loss spectra that have been normalized by dividing out  $I_E$ . The spectrum from the vertically aligned nanotube sample shows strong, regular oscillations with a period of about 4.25 eV, indicating regularity in the arrangement of nanotubes. The spectrum from the randomly oriented sample shows a weaker and less-periodic oscillation with a period of oscillation close to 3 eV. We can determine the spacing of the nanotubes in the vertically aligned sample by determining the oscillation period in reciprocal space using

$$\frac{\Delta k_{\text{out}}}{k_{\text{out}}} = \frac{\Delta E}{2E} \quad (6)$$

and

$$k_{\text{out}}^2 = \frac{2mE}{\hbar^2}, \quad (7)$$

where Eq. (6) is valid when  $\Delta E \ll E$ . If we further note that

$$\Delta \mathbf{K} = \Delta \mathbf{k}_{\text{out}} \quad (8)$$

and

$$d = \frac{2\pi}{|\Delta \mathbf{K}|}, \quad (9)$$

where  $d$  is the center-to-center spacing of the nanotubes, then we find that  $d = 52 \pm 12$  nm. This result is consistent with a recent TEM study by Zhang *et al.* for a similar sample.<sup>3</sup> Using TEM, they estimated that the diameter of the nanotubes ranged from 30 to 50 nm.<sup>3</sup> Of course, our result assumes that we were able to successfully divide out the factor  $I_E$ . Also, there are other issues regarding inelastic scattering that must be considered. For example, we have assumed that the energy-loss spectra were due to inelastic single scattering rather than inelastic rescattering of elastically diffracted electrons. We have also assumed that the inelastically scattered electrons retain coherence.<sup>11</sup>

#### IV. CONCLUSION

We have used reflection high-energy electron diffraction to determine the structure of the nanotubes in both aligned and nonaligned nanotube samples. The patterns roughly correspond to powder diffraction from graphite, but there is very little evidence of interlayer correlation. Furthermore, the ratio of the interlayer spacing to the in-plane nearest-neighbor distance was found to be larger than for ordered graphite. Also, from electron energy-loss spectra, we were able to estimate the center-to-center spacing of the nanotubes in the aligned sample to be  $52 \pm 12$  nm. This study demonstrates that RHEED can be a very powerful *in situ*, real-time tool for nanotube characterization.

#### ACKNOWLEDGMENTS

This work was supported by the NSF. J.T.D. would like to thank Michael McCarthy and W. Braun for valuable help with the design and construction of the energy filter. P.M.A., G.R., and B.Q.W. acknowledge funding from the Office of Naval Research (Grant No. N00014-00-1-0250) and the Focus Center New York for Interconnects at Rensselaer Polytechnic Institute.

<sup>1</sup>C. J. Lee, J. H. Han, J. E. Yoo, S. Y. Kang, J. H. Lee, and K.-I. Cho, *J. Korean Phys. Soc.* **37**, 858 (2000).

<sup>2</sup>K. Mukhopadhyay, A. Koshio, N. Tanaka, and H. Shinohara, *Jpn. J. Appl. Phys., Part 2* **37**, L1257 (1998).

<sup>3</sup>Z. J. Zhang, B. Q. Wei, G. Ramanath, and P. M. Ajayan, *Appl. Phys. Lett.* **77**, 3764 (2000).

<sup>4</sup>L. Jin, C. Bower, and O. Zhou, *Appl. Phys. Lett.* **73**, 1197 (1998).

<sup>5</sup>D. Reznik, C. H. Olk, D. A. Neumann, and J. R. D. Copley, *Phys. Rev. B* **52**, 116 (1995).

<sup>6</sup>O. Zhou, R. M. Fleming, D. W. Murphy, C. H. Chen, R. C. Haddon, A. P. Ramirez, and S. H. Glarum, *Science* **263**, 1744 (1994).

<sup>7</sup>Y. Saito, T. Yoshikawa, S. Bandow, M. Tomita, and T. Hayashi, *Phys. Rev. B* **48**, 1907 (1993).

<sup>8</sup>A. Burian, J. C. Dore, H. E. Fischer, and J. Sloan, *Phys. Rev. B* **59**, 1665 (1999).

<sup>9</sup>M. L. Terranova, S. Piccirillo, V. Sessa, P. Sbornicchia, M. Rossi, and S. Botti, *Mater. Chem. Phys.* **66**, 270 (2000).

<sup>10</sup>W. Braun, *Applied RHEED: Reflection High-Energy Electron Diffraction During Crystal Growth* (Springer-Verlag, New York, 1999).

<sup>11</sup>Zhong Lin Wang, *Elastic and Inelastic Scattering in Electron Diffraction and Imaging* (Plenum, New York, 1995).